

Should the Drift Chamber Inner Cylinder Be Load Bearing?

Abstract

Chamber endplates in which the inner and outer radii are at the same z coordinate (such as both endplates of the BABAR drift chamber) suffer large deflections under the wire load if they are only supported at the outer radius. By making the inner cylinder load bearing the deflections of the endplates would be reduced by a factor of ≈ 30 . This would permit the use of thinner endplates, or simplify the prestressing operation, or both. Of course, both the inner and outer cylinders must be stable against buckling under the wire load. Calculations indicate that a 540- μm -thick carbon-fiber inner cylinder would be just at the buckling limit, while a 1.5-mm-thick cylinder would buckle only at 10 times nominal load. A recent destructive test at Princeton supports these calculations. A 1.5-mm-thick inner cylinder would present 0.7% radiation lengths to particles, a modest increment to that of the adjacent PEP-II support tube (presently spec'ed to be 1.2% of a radiation length, not counting aluminum needed for an rf shield).

1 Deflection of Flat Annular Plates Under Uniform Loading

There exist analytic solutions to the deflections and stresses of flat circular endplates under uniform loads, summarized in the *Roark's Formulas for Stress and Strain* by W.C. Young (6th ed., McGraw Hill, 1989). These formulae are included as part of *TK Solver*, a PC-based engineering spreadsheet program (Universal Technical Systems, Rockford, IL, 815-963-2220).

We have used the formulae of Chapter 10, Table 24, Case 2 to calculate the measured deflections of several existing drift chambers, whose properties are surveyed in Table 1.

Among chambers with flat endplates, we calculated the deflections of the CLEO II, CDF and ZEUS chambers with results summarized on pages 8-10. The agreement is rather good using values of Young's modulus for aluminum reduced by the fraction of the endplate area lost to holes. The CLEO II endplate is supported only at its outer edge, while the CDF and ZEUS endplates are supported at both inner and outer radii.

Calculations for the proposed 32-mm-thick rear endplate of the BABAR drift chamber are presented on p. 11, with results very similar to those reported earlier by C. Hearty (who used the same formula from Roark and Young); namely a maximum deflection of 3.3 mm under a load of 3500 kg. The plate deforms into a very shallow cone of angle 5 mrad.

Table 1. Survey of Large Cylindrical Drift Chambers																			
	JADE	Mark II	TASSO	CLEO	ARGUS	Benichou	VENUS	Mark III	OPAL	SLD	CLEO II	Mark II	CDF	KEDR	AMY	ZEUS	BES	KLOE	
Reference	1	2	3	4	5	6	7	8	9	10	11	12	13	14	15	16	17	18	
Chamber size																			
R_min (mm)		373	320	172	150	400	250	140	250	200	175	192	277	125		162	155	~200	
R_max (mm)	800	1509	1280	950	859	1700	1260	1140	1850	1000	945	1519	1380	535	787	850	1150	1000	
L_max (mm)	3000	2692	3520	1930	2000	4500	3000	2340	4000	1800	2150	2300	3214	100	1792	2030	2120	3300	
Wire/cell parameters																			
Sense wires	1536	3204	2340	5304	5940	12880	7104	528	3816	5120	12240	5832	6156	1512	9048	4608	2808	~12000	
Other wires		9612	7020	15912	24588	64400	21312	1584	?	32640	36240	?	30448	14520	27144	19584	16572	~36000	
Total layers	48	16	15	17	36	40	29	62	159	80	51	72	72	56	40	72	40	~48	
Stereo layers		10	6	8	18	9	9	10		48	11	36	36	24	15	32	20	~24	
R_min (mm)		414	367	213	180		286	175		238	199	246	309		155	182	195		
R_max (mm)		1448	1222	892			1213			961	901	1448	1320		639	794	1095		
Geometry	jet	square	square	square	square	hex	square	rect.	jet	jet	square	jet	jet	jet	hex	jet	jet	square	
Max drift (mm)	70	18	16	6	18	10	10	30	250	30	7		40	30	6	25	31	15	
Min. resolution (micron)	150	150	220	210	150		150	250	110	55	100	125	200	40	140	100	200	~100	
dE/dx resolution (%)	10				5.6			15	3.5	7	7.1	7.2				6	9		
Endplates																			
Material	Rohacell	Al + H-C	Al	Al	Al	Al	Al	Al + H-C	Al	Al	Al	Al	Al	Al	GI-F	Al	Al	Al	Al or C-F
Thickness (mm)		76	35		30	5	21	76	28	5.1	31.8	50.8	50.8	21	30	20	40		
Geometry	flat + rib	flat + cone	flat	flat	flat	cone	sphere	flat	cone	parabola	flat	flat	flat	flat	stepped	flat	flat	sphere	
Wire load (tonnes)	1.2		2.3		3.1	33.7	6.8		14	13.3	6.8	20	25	3.4	4.5	5.9			
Max deflection (mm)		8				3	0.6		0.5		7.9		1.4	3		1.8		~1	
Outer cylinder																			
Material		Al	Al		Al	H-C	C-F	Al	Al	Al + H-C	Al + H-C	Al	Al	GI-F	Al	Al	Al	Al	rods
Thickness		6	6		6	25	5	6			8	12.7	6.4	5	posts	6	10		
Inner cylinder																			
Material		Lexan	GI-F		C-F	foil	C-F	paper	foil	Al + H-C	C-F	Be	C-F	C-F	Kevlar	Al + foam	C-F	foil	
Thickness		3	5		3.3		1	1			0.75	2	2	1.5	1	1.4 + 9	2		
Load bearing		no	yes			no	no	no	no	yes	no		yes		no	yes		no	
Stringing																			
Stringing		horiz.									vert.		horiz.				vert.		
Prestressing																			
Prestressing		rods								rods	rods		wires	external	rods	rods			
C-F - carbon-fiber/epoxy, GI-F = glass-fiber/epoxy, H-C = honeycomb																			

Then on p. 12 we show results assuming both the inner and outer edges of the plate are supported; in this case the maximum deflection is only 100 μm , and the 3500 kg load is distributed with 2100 kg at the outer edge and 1400 kg at the inner. A cross section of the plate is now a shallow parabola, and the angles at the edges are less than 1 mrad.

Thus the calculations indicate a factor of 28 reduction in the deflection of the flat endplate when both edges are supported compared to supporting only the outer edge.

A preliminary finite element analysis of the proposed biconical carbon-fiber endplate using the PC-based program ALGOR indicates a factor of 8 reduction in the maximum deflection when both edges are supported compared to supporting only the outer edge. Details of this analysis will be presented in a separate note.

The deflection of a flat plate is almost entirely due to bending (as contrasted with elongation), and so varies as $1/t^3$ where t is the thickness of the plate. For example, a 16-mm-thick plate would deflect by 0.8 mm.

The additional results on pp. 13-14 hold if the edge (or edges) of the plate are clamped

rather than simply supported as previously assumed. Clamping (= constraining the slope of the plate as well as the position) would reduce the deflection by an additional factor of 5.

However, the clamping condition is unrealistic if the endplate is simply attached to a thin-wall support tube; in practice the end of the support tube would provide very little resistance to the bending of 1-5 mrad at the edges of the endplate. A massive stiffening ring would be required to provide the clamping condition.

2 Buckling of a Cylindrical Shell Under Axial Load

If the proposed endplates were supported at both inner and outer edges the deflection under the wire load would be only 100-200 μm . This is so small that no prestressing of the endplates would be needed. This advantage would be best realized if both outer and inner support tubes were mounted together with the endplates before wire stringing, and the stringing performed with the chamber axis vertical (as for the CLEO II and ZEUS chambers).

A critical issue is the thickness of the inner support tube so that it is stable against buckling.

A well-known result for long columns is the Euler condition for the maximum axial force before the column deforms into an arc (picturesquely demonstrated by Charlie Chaplin's cane):

$$F_{\max} = \frac{4\pi^2 EI}{l^2}, \quad (\text{Euler})$$

where E is the modulus of elasticity (Young's modulus), I is the area moment of inertia, and l is the length. For a tube of radius r and thickness t the moment of inertia is $I = \pi r^3 t$, so we have

$$F_{\max} = \frac{4\pi^3 E r^3 t}{l^2}, \quad (\text{tube}).$$

For solid columns Euler calculated that buckling into higher-order modes required a larger axial force than that for the fundamental mode just presented. Around 1910, Lorenz, and also Timoshenko, realized that for thin-walled tubes it is easier to buckle into a higher-order mode. They first considered modes corresponding to longitudinal waves and later considered combined longitudinal and azimuthal waves to find in both cases that

$$F_{\max} = \frac{2\pi E t^2}{\sqrt{3(1 - \nu^2)}}, \quad (\text{Timoshenko}),$$

where ν is Poisson's ratio (the ratio of transverse to longitudinal strain of a material under longitudinal stress). This result is remarkable in that neither the length nor the radius of the tube appears. The characteristic wavelength of the failure mode is small compared to both the length and radius of the tube, in contrast to Euler's result for solid columns.

The failure mode for combined longitudinal and azimuthal modes is sometimes called the Yoshimura pattern, illustrated in the figure on p. 4 (taken from *Buckling of Shells for Engineers* by L. Kollár and E. Dulácska, Wiley, 1984). In this pattern the surface of the tube breaks up into flat triangular facets. Experiment shows that the Yoshimura pattern is the typical failure mode for thin tubes.

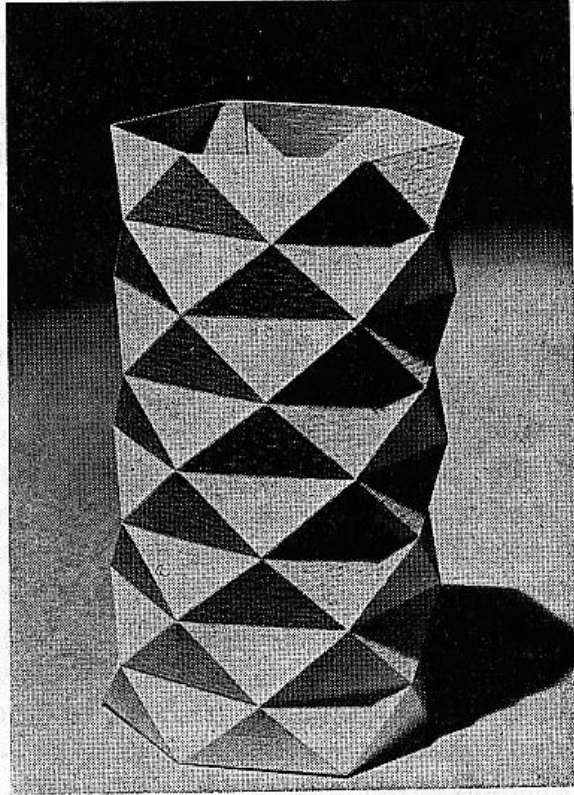


Fig. 2.6. The Yoshimura-pattern

However, experiment also shows that the force at which buckling occurs is typically less than that given by Timoshenko's result, especially for long thin tubes. Some data are summarized in the figure at the top of p. 5 (taken from *Buckling of Bars, Plates, and Shells* by D.O. Brush and B.O. Almroth, McGraw-Hill, 1975). Here $k_a \equiv F_{\max} l^2 (1 - \nu^2) / (2\pi r t^3 E)$, $a \equiv r$ and $h \equiv t$. A number of explanations for this discrepancy have been put forward, but it is very suggestive that the experimental data for buckling under axial compression appear to follow the functional form of theory (and experiment) for buckling under torsion. See the lower figure on p. 5. The buckling may be provoked by a slight torsion due to asymmetric loading or imperfection in the tube. Therefore I adopt the semi-empirical functional form

$$F_{\max} = \frac{\pi^3 E t^{9/4} r^{1/4}}{6 l^{1/2} (1 - \nu^2)^{5/8}}, \quad (\text{semi-empirical}),$$

which is a translation of the fit $k_a = Z^{3/4}$ to the data on both axial and torsional buckling.

2.1 Laboratory Test

The buckling force predicted by the above formula is remarkably large. We felt the need to perform a lab test to check it.

We rolled a cylinder of radius 6" and length 36" from a sheet of G-10 about 0.018" = 450 μm thick. The seam of the tube consisted of a 1" overlap secured with pop rivets every

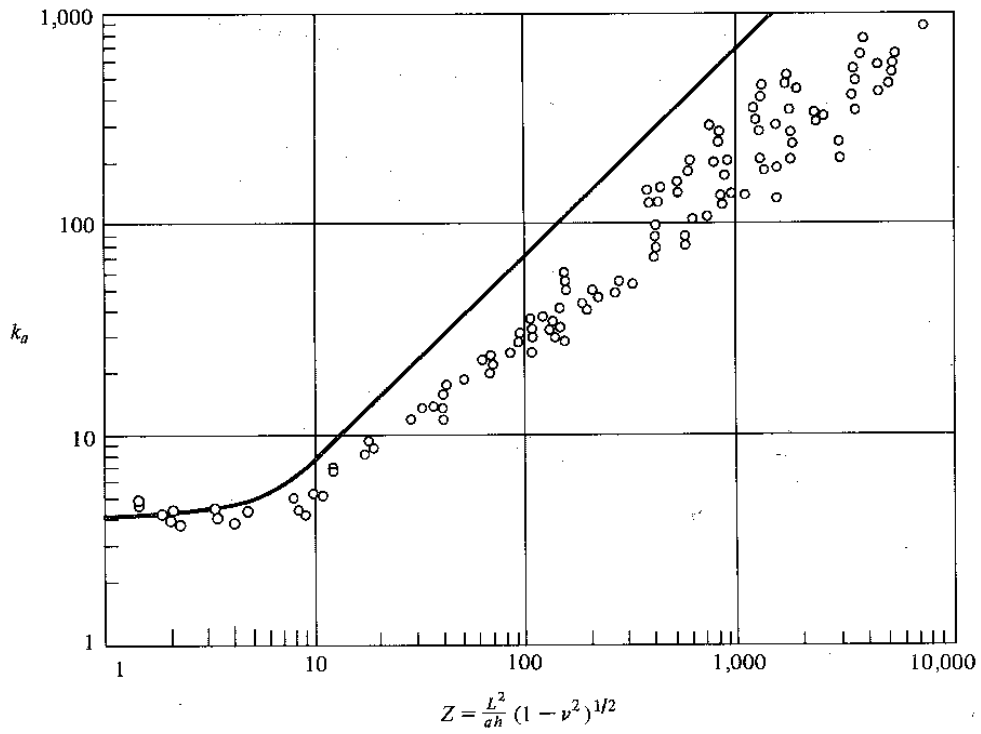


FIGURE 5.14
Comparison of theoretical and experimental values for cylinders subjected to axial compression.

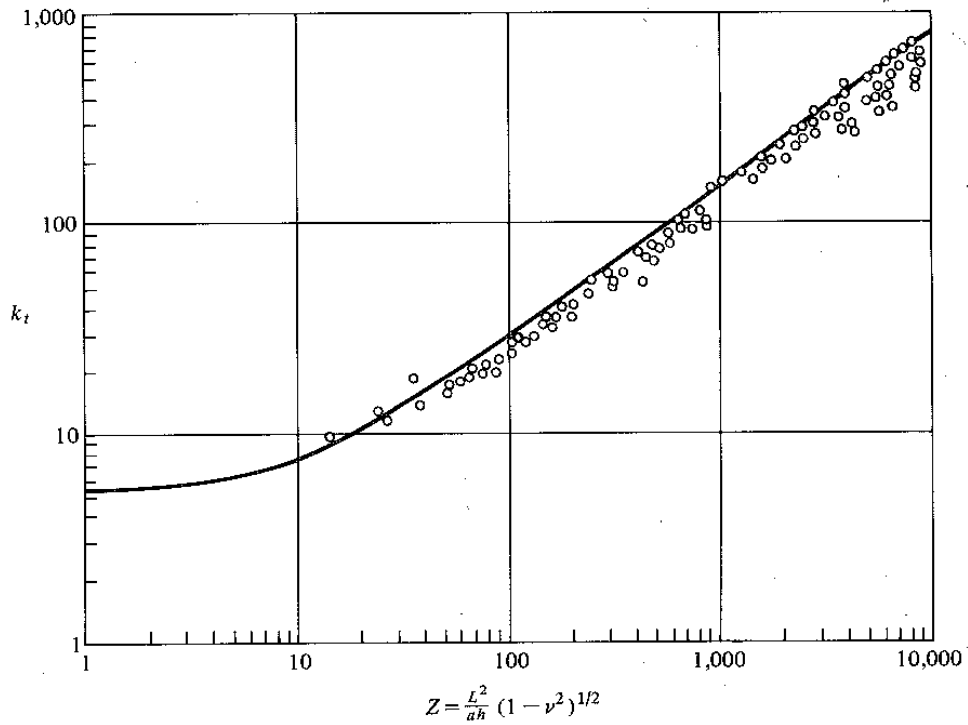


FIGURE 5.15
Comparison of theoretical and experimental values for cylinders subjected to torsion.

inch. A data sheet lists the modulus of G-10 as 2.5×10^6 psi. We assume the Poisson ratio is 0.3. The calculated buckling force is then 425 pounds.

We placed a plate on the top end of the tube and carefully added lead bricks until the tube buckled – at a load of 715 pounds! The failure pattern was of the Yoshimura type, but restricted to the upper and lower 1/5 of the tube. See the photo below.



We thus obtain some confidence that the semi-empirical formula represents a lower bound on the buckling force for tubes similar to that proposed for BABAR.

2.2 Proposal for the BABAR Drift Chamber

The support tubes for the BABAR chamber are to be made of filament-wound carbon-fiber epoxy. Tubes fabricated from this material can be obtained with a Young's modulus at least 1.4×10^{11} Pascals. We take the Poisson ratio to be 0.3.

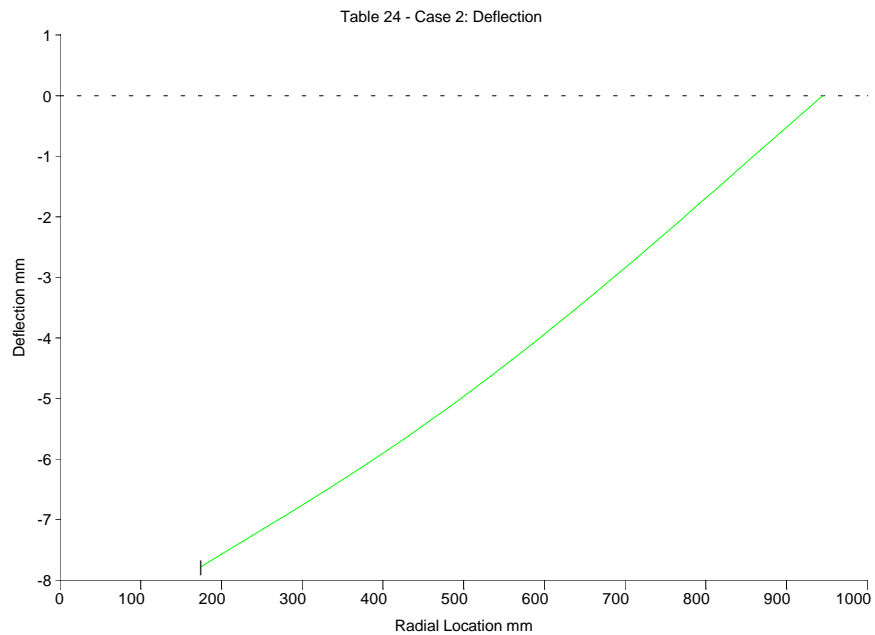
According to the calculations in sec. 1, the 3500-kg wire load should be distributed with 2100 kg on the outer tube and 1400 kg on the inner tube for minimum deflection of the rear endplate.

Then according to the semi-empirical formula, the thickness of 3-mm-long tubes just at the buckling limit is $540 \mu\text{m}$ for the inner tube, and $570 \mu\text{m}$ for the outer tube. For safety **we design the buckling load to be 10 times the nominal load**, requiring tubes 2.8 times thicker: **1.5 mm thick for the inner tube and 1.6 mm thick for the outer tube.**

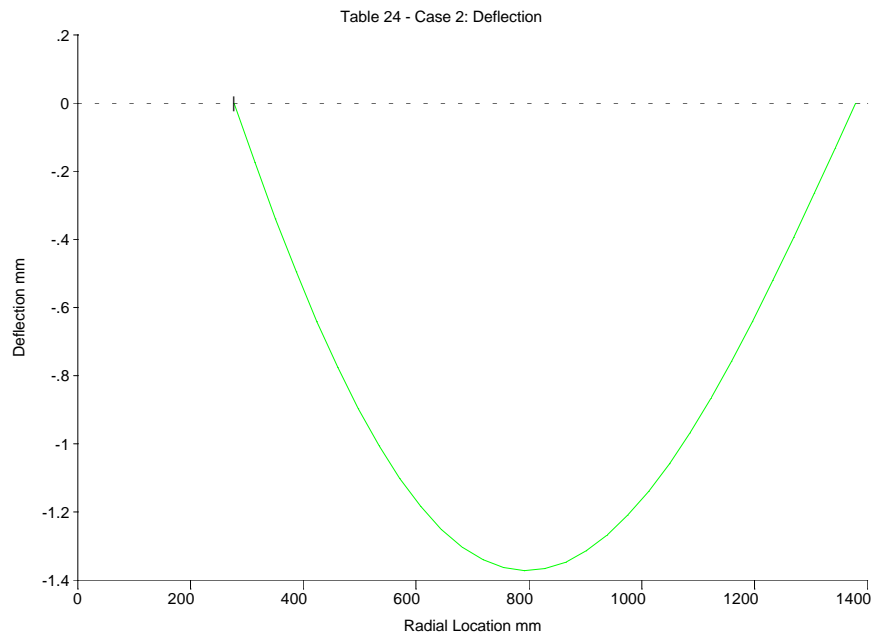
3 References

- [1] W. Farr *et al.*, *A Drift Chamber System for the Detection of Narrow Particle Jets from e^+e^- Reactions*, Nucl. Instr. and Meth. **156** (1978) 283; H. Drumm *et al.*, *Experience with the Jet Chamber of the JADE Detector at PETRA*, Nucl. Instr. and Meth. **176** (1980) 333.
- [2] W. Davies-White *et al.*, *A Large Cylindrical Drift Chamber for the Mark II Detector at Spear*, Nucl. Instr. and Meth. **160** (1979) 227.
- [3] H. Boerner *et al.*, *The Large Cylindrical Drift Chamber of TASSO*, Nucl. Instr. and Meth. **176** (1980) 151.
- [4] D. Andrews *et al.*, *The CLEO Detector*, Nucl. Instr. and Meth. **211** (1983) 47.
- [5] M. Danilov *et al.*, *The Argus Drift Chamber*, Nucl. Instr. and Meth. **217** (1983) 153.
- [6] J.L. Bénichou *et al.*, *Design Study of a Large Cylindrical Drift Chamber*, Nucl. Instr. and Meth. **217** (1983) 163.
- [7] R. Arai *et al.*, *Development of a Large Cylindrical Drift Chamber for the VENUS Detector at TRISTAN*, Nucl. Instr. and Meth. **217** (1983) 181.
- [8] J. Roehrig *et al.*, *The Central Drift Chamber for the Mark III Detector at SPEAR*, Nucl. Instr. and Meth. **26** (1984) 319.
- [9] H.J. Burckhart *et al.*, *Investigation of Very Long Jet Chambers*, Nucl. Instr. and Meth. **A244** (1986) 416; H.M. Fischer *et al.*, *The OPAL Jet Chamber Full Scale Prototype*, Nucl. Instr. and Meth. **A252** (1986) 331; R.D Heuer and A. Wagner, *The OPAL Jet Chamber*, Nucl. Instr. and Meth. **A265** (1988) 11.
- [10] W.B. Atwood *et al.*, *Performance of the SLD Central Drift Chamber Prototype*, Nucl. Instr. and Meth. **A252** (1986) 295; M.J. Fero *et al.*, *Performance of the SLD Central Drift Chamber*, Nucl. Instr. and Meth. **A367** (1995) 111.
- [11] D.G. Cassel *et al.*, *Design and Construction of the CLEO II Drift Chamber*, Nucl. Instr. and Meth. **A252** (1986) 325; Y. Kubota *et al.*, *The CLEO II Detector*, Nucl. Instr. and Meth. **A320** (1992) 66.
- [12] Gail G. Hanson, *The New Drift Chamber for the Mark II Detector at the SLAC Linear Collider*, Nucl. Instr. and Meth. **A252** (1986) 343; G. Abrams *et al.*, *The Mark II Detector for the SLC*, Nucl. Instr. and Meth. **A281** (1989) 55.
- [13] F. Bedeschi *et al.*, *Design and Construction of the CDF Central Tracking Chamber*, Nucl. Instr. and Meth. **A268** (1988) 50.
- [14] S.E. Baru *et al.*, *The KEDR Drift Chamber*, Nucl. Instr. and Meth. **A323** (1992) 151.
- [15] K. Ueno *et al.*, *The Design of the AMY Central Drift Chamber and Performance in a 3 T Magnetic Field*, Nucl. Instr. and Meth. **A323** (1992) 601.
- [16] B. Foster *et al.*, *The Design and Construction of the ZEUS Central Tracking Detector*, Nucl. Instr. and Meth. **A338** (1994) 254.
- [17] J.Z Bai *et al.*, *The BES Detector*, Nucl. Instr. and Meth. **A344** (1994) 319.
- [18] A. Calcaterra, *The KLOE Drift Chamber*, Nucl. Instr. and Meth. **A367** (1995) 104.

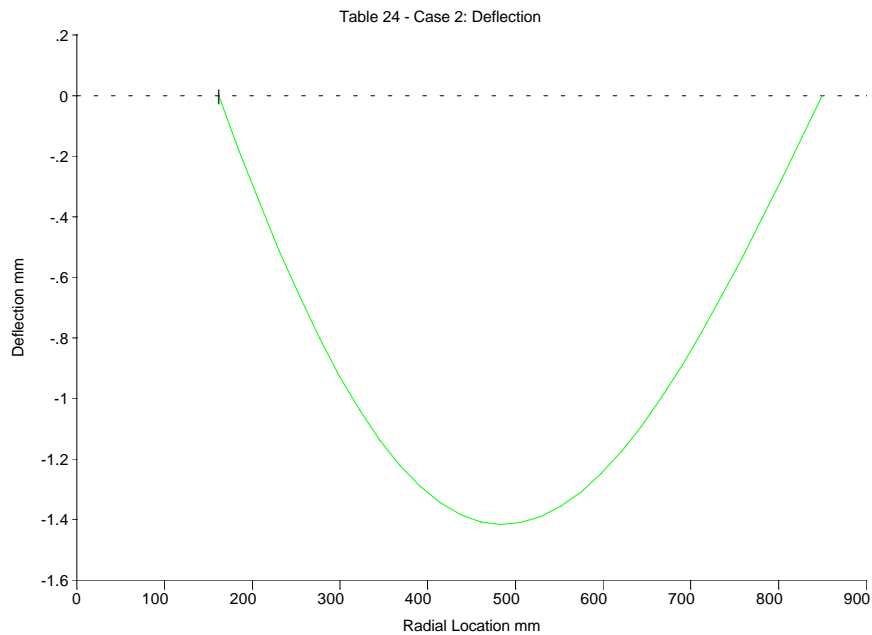
St	Input	Name	Output	Unit	Comment
					CLEO II endplate, supported at outer edge
					Table 24 - Roark & Young (6 ed) [file tab24.tk] Formulas for flat circular plates of [mod by ktm] constant thickness [file 242.tk also mod]
		case	'Case_2a		Reference number
4	matnum	matl	"Aluminum		Material Number (See Material Table) Material name
6.205E10	E	nu	.3	Pa	Young's Modulus (reduced 10% for holes) Poisson's ratio
.945	a			m	Outer Radius
.175	b			m	Inner Radius
	Area		2.7093095	m^2	Area of plate
.032	t			m	Plate Thickness
6800	L			kgf	Load on plate
	q		24596.673	Pa	Uniformly distributed pressure
	D		186195.46	N-m	Plate Constant + $E*t^3/12/(1-\nu^2)$
					AT OUTER EDGE:
	ya		0	m	Deflection
	tha		.0115536	rad	Radial Slope Angle
	Mra		0	N-m/m	Radial Bending Moment
	Qa		-11223.37	N/m	Shear Force Density
	La		-6800	kgf	Shear Force
					AT INNER EDGE:
	yb		-.0077753	m	Deflection
	thb		.008407	rad	Radial Slope Angle
	Mrb		0	N-m/m	Radial Bending Moment
	Qb		0	N/m	Shear Force Density
	Lb		0	kgf	Shear Force



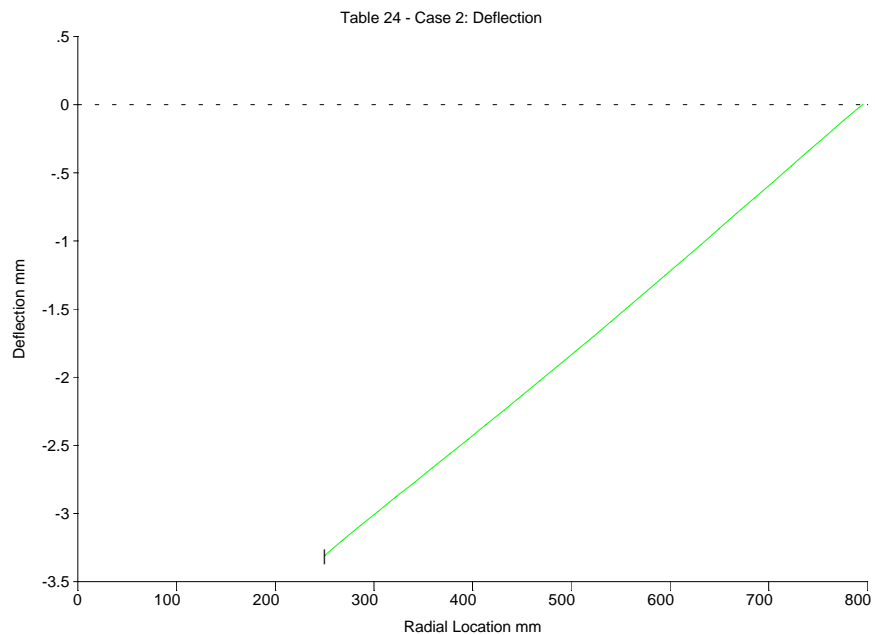
St	Input	Name	Output	Unit	Comment
					CDF endplate, supported both edges
					Table 24 - Roark & Young (6 ed) [file tab24.tk] Formulas for flat circular plates of [mod by ktm] constant thickness [file 242.tk also mod]
		case	'Case_2c		Reference number
4	matnum				Material Number (See Material Table)
	matl		"Aluminum		Material name
4.234E10	E			Pa	Young's Modulus (reduced 30% for holes)
	nu		.3		Poisson's ratio
1.38	a			m	Outer Radius
.277	b			m	Inner Radius
	Area		5.7417978	m^2	Area of plate
5.08E-2	t			m	Plate Thickness
25000	L			kgf	Load on plate
	q		42669.563	Pa	Uniformly distributed pressure
	D		508299.11	N-m	Plate Constant + $E*t^3/12/(1-\nu^2)$
					AT OUTER EDGE:
	ya		0	m	Deflection
	tha		.0035897	rad	Radial Slope Angle
	Mra		0	N-m/m	Radial Bending Moment
	Qa		-17425.02	N/m	Shear Force Density
	La		-15417.22	kgf	Shear Force
					AT INNER EDGE:
	yb		0	m	Deflection
	thb		-.004833	rad	Radial Slope Angle
	Mrb		0	N-m/m	Radial Bending Moment
	Qb		53958.252	N/m	Shear Force Density
	Lb		9582.7781	kgf	Shear Force



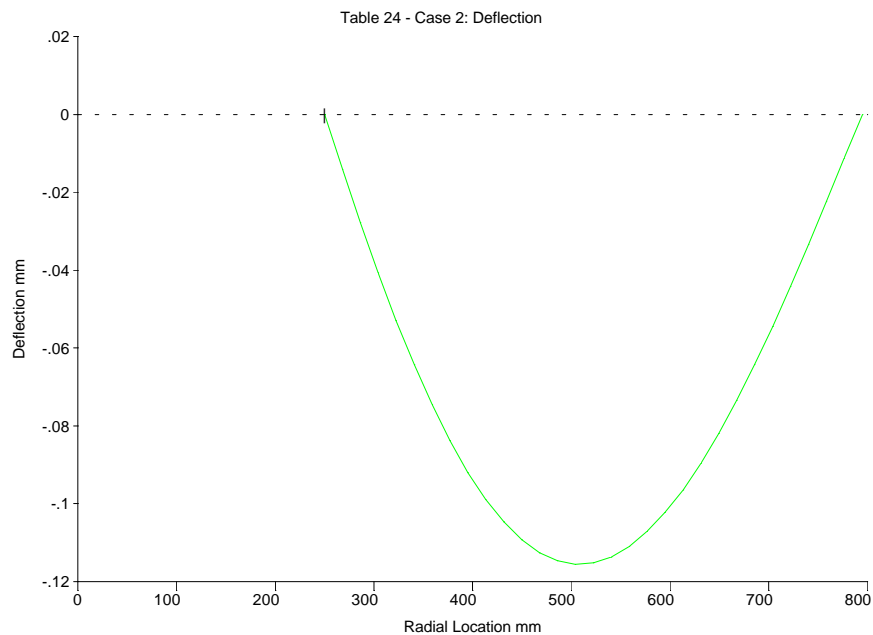
St	Input	Name	Output	Unit	Comment
					ZEUS endplate, supported both edges
					Table 24 - Roark & Young (6 ed) [file tab24.tk] Formulas for flat circular plates of [mod by ktm] constant thickness [file 242.tk also mod]
		case	'Case_2c		Reference number
4	matnum	matl	"Aluminum		Material Number (See Material Table) Material name
6.339E10	E	nu	.3	Pa	Young's Modulus (reduced 8% for holes) Poisson's ratio
.85	a			m	Outer Radius
.162	b			m	Inner Radius
	Area		2.1873527	m^2	Area of plate
.02	t			m	Plate Thickness
6000	L			kgf	Load on plate
	q		26881.81	Pa	Uniformly distributed pressure
	D		46439.56	N-m	Plate Constant + $E*t^3/12/(1-\nu^2)$
					AT OUTER EDGE:
	ya		0	m	Deflection
	tha		.0059379	rad	Radial Slope Angle
	Mra		0	N-m/m	Radial Bending Moment
	Qa		-6799.849	N/m	Shear Force Density
	La		-3705.715	kgf	Shear Force
					AT INNER EDGE:
	yb		0	m	Deflection
	thb		-.0080245	rad	Radial Slope Angle
	Mrb		0	N-m/m	Radial Bending Moment
	Qb		22089.13	N/m	Shear Force Density
	Lb		2294.2853	kgf	Shear Force



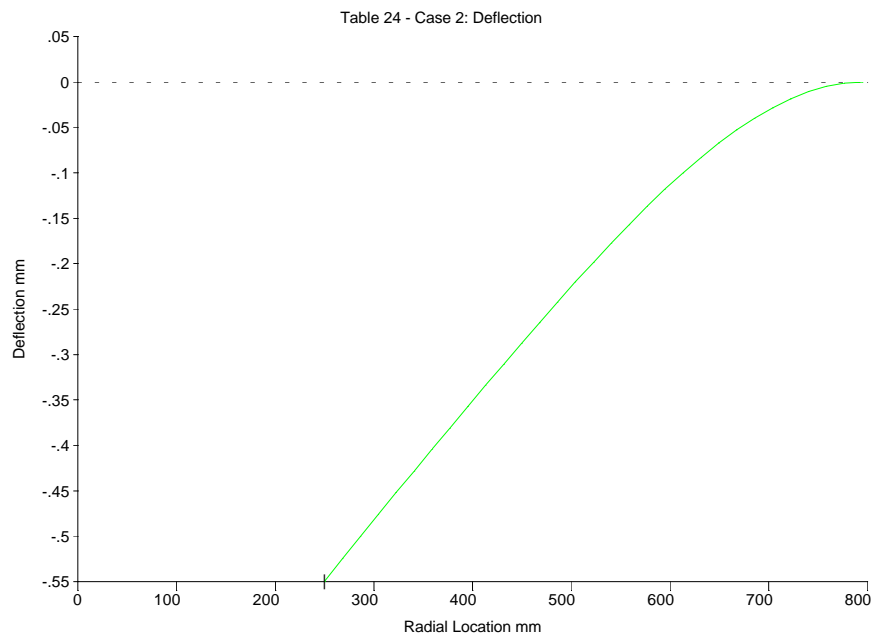
St	Input	Name	Output	Unit	Comment
					BABAR rear endplate, supported at outer edge
					Table 24 - Roark & Young (6 ed) [file tab24.tk] Formulas for flat circular plates of [mod by ktm] constant thickness [file 242.tk also mod]
		case	'Case_2a		Reference number
4	matnum				Material Number (See Material Table)
	matl	"Aluminum			Material name
5.857E10	E			Pa	Young's Modulus (reduced 15% for holes)
	nu	.3			Poisson's ratio
.795	a			m	Outer Radius
.25	b			m	Inner Radius
	Area	1.7892156		m ²	Area of plate
.032	t			m	Plate Thickness
3500	L			kgf	Load on plate
	q	19170.412		Pa	Uniformly distributed pressure
	D	175752.91		N-m	Plate Constant + $E \cdot t^3 / 12 / (1 - \nu^2)$
	ya	0		m	AT OUTER EDGE: Deflection
	tha	.0061928		rad	Radial Slope Angle
	Mra	0		N-m/m	Radial Bending Moment
	Qa	-6866.685		N/m	Shear Force Density
	La	-3500		kgf	Shear Force
	yb	-.0033073		m	AT INNER EDGE: Deflection
	thb	.0060856		rad	Radial Slope Angle
	Mrb	0		N-m/m	Radial Bending Moment
	Qb	0		N/m	Shear Force Density
	Lb	0		kgf	Shear Force



St	Input	Name	Output	Unit	Comment
					BABAR rear endplate, supported both edges
					Table 24 - Roark & Young (6 ed) [file tab24.tk] Formulas for flat circular plates of [mod by ktm] constant thickness [file 242.tk also mod]
		case	'Case_2c		Reference number
4		matnum			Material Number (See Material Table)
		matl	"Aluminum		Material name
5.857E10		E		Pa	Young's Modulus (reduced 15% for holes)
		nu	.3		Poisson's ratio
.795		a		m	Outer Radius
.25		b		m	Inner Radius
		Area	1.7892156	m ²	Area of plate
.032		t		m	Plate Thickness
3500		L		kgf	Load on plate
		q	19170.412	Pa	Uniformly distributed pressure
		D	175752.91	N-m	Plate Constant + $E \cdot t^3 / 12 / (1 - \nu^2)$
		ya	0	m	AT OUTER EDGE: Deflection
		tha	6.1746E-4	rad	Radial Slope Angle
		Mra	0	N-m/m	Radial Bending Moment
		Qa	-4127.383	N/m	Shear Force Density
		La	-2103.758	kgf	Shear Force
		yb	0	m	AT INNER EDGE: Deflection
		thb	-.0007872	rad	Radial Slope Angle
		Mrb	0	N-m/m	Radial Bending Moment
		Qb	8710.98	N/m	Shear Force Density
		Lb	1396.2424	kgf	Shear Force



St	Input	Name	Output	Unit	Comment
					BABAR rear endplate, clamped at outer edge
					Table 24 - Roark & Young (6 ed) [file tab24.tk] Formulas for flat circular plates of [mod by ktm] constant thickness [file 242.tk also mod]
		case	'Case_2e		Reference number
4		matnum			Material Number (See Material Table)
		matl	"Aluminum		Material name
5.857E10		E		Pa	Young's Modulus (reduced 15% for holes)
		nu	.3		Poisson's ratio
.795		a		m	Outer Radius
.25		b		m	Inner Radius
		Area	1.7892156	m ²	Area of plate
.032		t		m	Plate Thickness
3500		L		kgf	Load on plate
		q	19170.412	Pa	Uniformly distributed pressure
		D	175752.91	N-m	Plate Constant + $E \cdot t^3 / 12 / (1 - \nu^2)$
		ya	0	m	AT OUTER EDGE: Deflection
		tha	0	rad	Radial Slope Angle
		Mra	-1354.952	N-m/m	Radial Bending Moment
		Qa	-6866.685	N/m	Shear Force Density
		La	-3500	kgf	Shear Force
		yb	-.0005495	m	AT INNER EDGE: Deflection
		thb	.0013849	rad	Radial Slope Angle
		Mrb	0	N-m/m	Radial Bending Moment
		Qb	0	N/m	Shear Force Density
		Lb	0	kgf	Shear Force



St	Input	Name	Output	Unit	Comment
					BABAR rear endplate, clamped both edges
					Table 24 - Roark & Young (6 ed) [file tab24.tk] Formulas for flat circular plates of [mod by ktm] constant thickness [file 242.tk also mod]
		case	'Case_2h		Reference number
4		matnum			Material Number (See Material Table)
		matl	"Aluminum		Material name
5.857E10		E		Pa	Young's Modulus (reduced 15% for holes)
		nu	.3		Poisson's ratio
.795		a		m	Outer Radius
.25		b		m	Inner Radius
		Area	1.7892156	m ²	Area of plate
.032		t		m	Plate Thickness
3500		L		kgf	Load on plate
		q	19170.412	Pa	Uniformly distributed pressure
		D	175752.91	N-m	Plate Constant + $E \cdot t^3 / 12 / (1 - \nu^2)$
		ya	0	m	AT OUTER EDGE: Deflection
		tha	0	rad	Radial Slope Angle
		Mra	-405.247	N-m/m	Radial Bending Moment
		Qa	-4384.885	N/m	Shear Force Density
		La	-2235.008	kgf	Shear Force
		yb	0	m	AT INNER EDGE: Deflection
		thb	0	rad	Radial Slope Angle
		Mrb	-651.361	N-m/m	Radial Bending Moment
		Qb	7892.124	N/m	Shear Force Density
		Lb	1264.9917	kgf	Shear Force

